

Discovery of Arylsulfonamide Na_v1.7 Inhibitors: IVIVC, MPO Methods, and Optimization of Selectivity Profile

Anthony J. Roecker,* Mark E. Layton, Joseph E. Pero, Michael J. Kelly, III, Thomas J. Greshock, Richard L. Kraus, Yuxing Li, Rebecca Klein, Michelle Clements, Christopher Daley, Aneta Jovanovska, Jeanine E. Ballard, Deping Wang, Fuqiang Zhao, Andrew P. J. Brunskill, Xuanjia Peng, Xiu Wang, Haiyan Sun, Andrea K. Houghton, and Christopher S. Burgey

Cite This: *ACS Med. Chem. Lett.* 2021, 12, 1038–1049

Read Online

ACCESS |

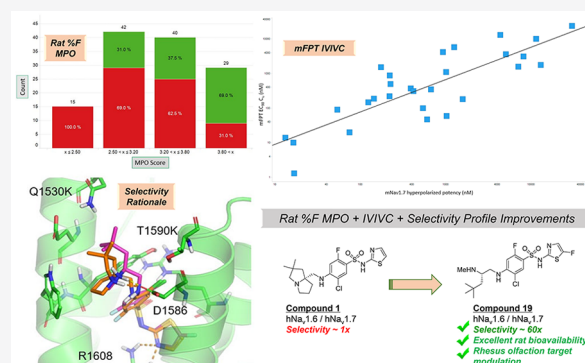
Metrics & More

Article Recommendations

Supporting Information

ABSTRACT: The voltage-gated sodium channel Na_v1.7 continues to be a high-profile target for the treatment of various pain afflictions due to its strong human genetic validation. While isoform selective molecules have been discovered and advanced into the clinic, to date, this target has yet to bear fruit in the form of marketed therapeutics for the treatment of pain. Lead optimization efforts over the past decade have focused on selectivity over Na_v1.5 due to its link to cardiac side effects as well as the translation of preclinical efficacy to man. Inhibition of Na_v1.6 was recently reported to yield potential respiratory side effects preclinically, and this finding necessitated a modified target selectivity profile. Herein, we report the continued optimization of a novel series of arylsulfonamide Na_v1.7 inhibitors to afford improved selectivity over Na_v1.6 while maintaining rodent oral bioavailability through the use of a novel multiparameter optimization (MPO) paradigm. We also report *in vitro*–*in vivo* correlations from Na_v1.7 electrophysiology protocols to preclinical models of efficacy to assist in projecting clinical doses. These efforts produced inhibitors such as compound 19 with potency against Na_v1.7, selectivity over Na_v1.5 and Na_v1.6, and efficacy in behavioral models of pain in rodents as well as inhibition of rhesus olfactory response indicative of target modulation.

KEYWORDS: Na_v1.7, Na_v1.6, ion channel, pain, arylsulfonamide, selectivity, olfaction



The discovery and development of novel nonopioid pain medications has been highlighted as a critical area of unmet medical need in recent years with a number of high-profile reviews and popular articles covering the topic.¹ The strong level of genetic validation for the voltage-gated sodium channel Na_v1.7 as a novel, nonopioid target for pain relief has afforded an enormous amount of effort in the scientific community focused on the discovery of potent and selective inhibitors of this channel.² Multimodality efforts across industry and academic groups have produced a number of clinical candidates advancing toward or into human studies.³ However, no selective Na_v1.7 inhibitors have demonstrated clinical efficacy in chronic or acute human pain conditions to date.⁴ This clinical experience has left the scientific field to ponder whether the ligands studied owned the necessary profiles to adequately test the mechanism regarding target engagement or if the translation of the human genetic condition into therapeutics was possible via the current approaches.⁵ Increasing target inhibition relative to what has been currently achieved in clinical study would add value toward validating or invalidating this important target.

The difficulty with increasing degree of channel blockade relates to the requisite increase in selectivity profile over homologous Na_v1.x channels necessary to safely interrogate this hypothesis. High levels of selectivity over Na_v1.4 and Na_v1.5 blockade, inhibition of which affords known skeletal muscle and cardiac toxicity, respectively, have been achieved within the arylsulfonamide class of Na_v1.7 inhibitors represented by compounds 1, 2, and 3 as reported previously (Table 1).⁶ Lack of central inhibition of Na_v1.1 and Na_v1.2 has been achieved via limiting CNS penetration with this class of zwitterionic Na_v1.7 blocker, affording some safety margin to established CNS-related toxicities.⁷ However, recent studies from our laboratory revealed significant respiratory inhibition findings potentially related to Na_v1.6 blockade in the phrenic

Received: April 19, 2021

Accepted: May 26, 2021

Published: June 1, 2021

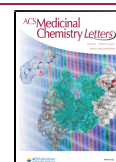
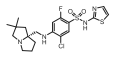
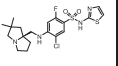
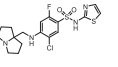


Table 1. Mouse Formalin Paw Efficacy and Mouse Na_v1.7 Inhibition Relationships under Depolarized and Hyperpolarized Assay Protocols

Structure			
Compound	1	2	3
Mouse Na _v 1.7 IC ₅₀ (de- / hyperpolarized μM) ^a	0.013 / 0.22	0.018 / 5.0	0.015 / 0.39
mFPT IC ₉₀ C _u (μM) ^b	0.22	3.6*	0.37
mPFT IC ₉₀ C _{p,u} / mouse depol. IC ₅₀	17	200	25
mPFT IC ₉₀ C _{p,u} / mouse hyper. IC ₅₀	1.0	0.7	0.9
Human Na _v 1.7 / 1.6 IC ₅₀ (μM) ^c	0.10 / 0.09	1.8 / 4.7	0.12 / 0.06

^aEstimated depolarized or hyperpolarized state potency as measured by PatchXpress in HEK293 cells stably expressing mouse Na_v1.7. IC₅₀ values are estimated from ≥3 cellular measurements at varying compound concentrations and standard deviation <50% of average value shown. ^bMouse formalin paw test performed as described in ref 22. ^cEstimated hyperpolarized state potency as measured by Qube in HEK293 cells stably expressing human Na_v1.7 or Na_v1.6; IC₅₀ values are estimated from ≥3 cellular measurements at varying compound concentrations; * = estimated value.

nerve, thus necessitating optimization of selectivity over this related channel.⁸ Notably, published compounds **1**, **2**, and **3** have limited to no selectivity over Na_v1.6 (Table 1). To address the potential increase in channel blockade necessary for efficacy, our efforts focused on establishing *in vitro*–*in vivo* correlations (IVIVC) between Na_v1.7 potency in different assay protocols to effects in a behavioral model of pain efficacy and a rhesus model of target modulation. The result of these efforts would give us a method to effectively assess increases in on-target potency *in vitro* related to pharmacodynamic endpoints. Our efforts also targeted establishing SAR in the arylsulfonamide series that significantly increased selectivity over Na_v1.6 to widen our therapeutic index.

Compounds **1**, **2**, and **3** in Table 1 were previously reported examples of arylsulfonamide Na_v1.7 blockers that display state-dependent channel inhibition. Previous potency values have been reported using a depolarized assay protocol, which placed the channel in a population of states that favor the inactivated state.⁹ All three compounds have very similar mouse potency in this assay protocol with IC₅₀ values of 13, 18, and 15 nM, respectively. These compounds were studied in a number of assay protocols including a hyperpolarized assay protocol, which placed the channel in a population of states favoring the resting state. Under this protocol, the mouse potency shifted significantly from 17- and 26-fold for **1** and **3** to more than 270-fold in the case of compound **2**. All three compounds were evaluated for efficacy in the mouse formalin paw test (mFPT) model, and the unbound concentration in plasma necessary for 90% reversal of the phase 2 effect was related to *in vitro* potency measures. While shifts were high (17–200-fold) relating phase 2 mFPT efficacy concentrations to depolarized potency, the ratios of mFPT efficacy to hyperpolarized potency were almost unity in all three cases. Notably, this ratio was able to distinguish potency differences between enantiomers **1** and **2** with similar depolarized potency values but disparate hyperpolarized potency values.¹⁰ Figure 1 demonstrates the relationship between hyperpolarized Na_v1.7 mouse potency and unbound concentration for 90% mFPT efficacy across a wide range of potency values within the arylsulfonamide series with an R² of 0.68. The hyperpolarized assay protocol was also evaluated for Na_v1.6, and this value was found to approximate the unbound concentrations necessary for measurable respiratory findings in rodents.⁸ With this data in hand, the Na_v1.7 and Na_v1.6 hyperpolarized assay protocols were utilized for further optimization of potency and selectivity.

The hyperpolarized potency values for human Na_v1.6 and Na_v1.7 for compounds **1**, **2**, and **3** are displayed at the bottom of Table 1. All compounds have limited to inverted selectivity over Na_v1.6, necessitating additional SAR to provide analogues with improved profiles for program advancement. While rodent bioavailability was not an issue for analogues **1**–**3**, limited rat oral bioavailability in the arylsulfonamide class was an issue identified across a variety of analogues in zwitterionic space, potentially due to low permeability.¹¹ An optimization approach was taken to establish SAR to improve selectivity

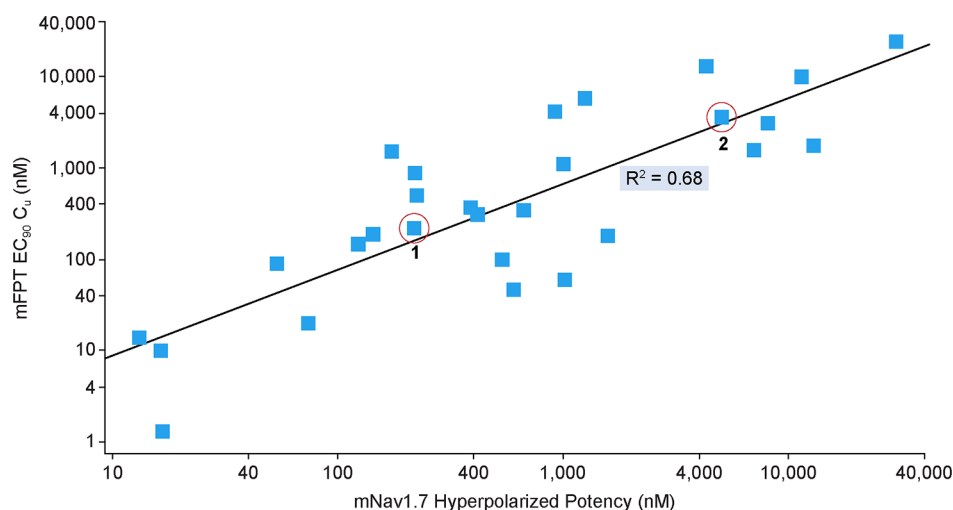


Figure 1. *In vitro*–*in vivo* correlation between mouse formalin paw test and mouse Na_v1.7 potency under hyperpolarized assay protocol.

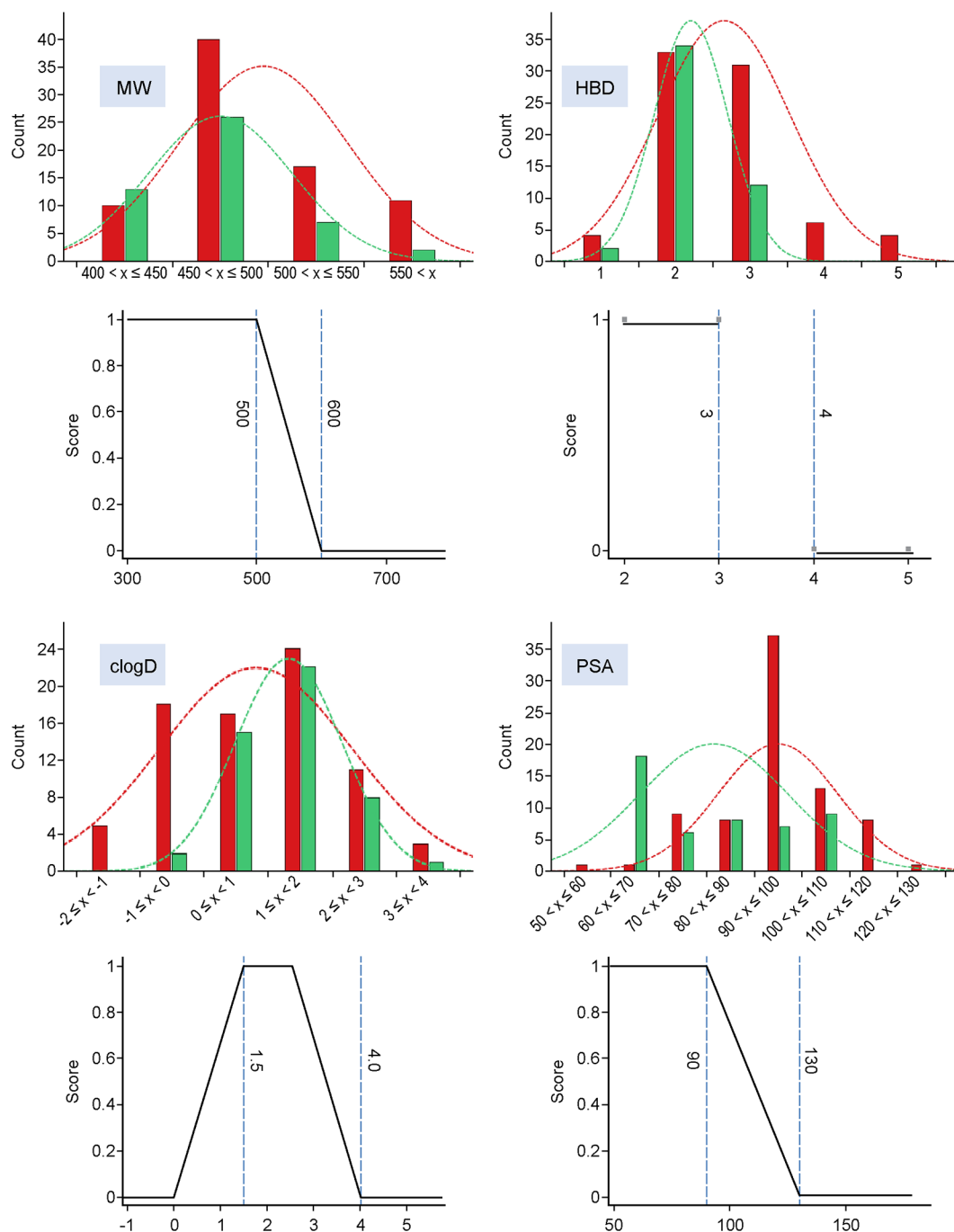


Figure 2. Distribution of properties (MW, HBD, cLogD, and PSA; Y axis = compound count) of analogues evaluated in rat oral PK studies ($\%F \geq 20\%$, green; $\%F < 20\%$, red) and property functions comprising custom oral bioavailability MPO paradigm.

over $\text{Na}_v1.6$ while concomitantly exploring space enriched for significant rodent oral bioavailability. A range of physicochemical properties were evaluated to determine potential values that could increase enrichment for rat oral bioavailability within this zwitterionic space for utility in prospective design. The results of four properties with the best enrichment data are shown in Figure 2.

Oral bioavailability (defined as rat $\%F \geq 20\%$: green bars $\geq 20\%$ and red bars $< 20\%$) was generally enriched with reductions in molecular weight (MW), limiting H-bond donor (HBD) count, balancing cLogD in a desirable range, and lowering polar surface area (PSA). These findings were aggregated into a simple four-point scoring system, with each

property given a score of 1. The scoring functions are depicted in Figure 2, with a monotonic declining function for MW and PSA, a step function for HBD, and a hump function for cLogD.¹² Enrichment in rat bioavailability utilizing this multiparameter optimization (MPO) paradigm is shown in Figure 3. Increased enrichment was observed upon increasing MPO score, with molecules scoring below 2.5, all exhibiting $< 20\%$ rat oral bioavailability. Increasing bioavailability enrichment was observed between 2.5 and 3.8, and significant enrichment was observed with scores > 3.8 , with almost 70% of compounds owning significant bioavailability. Compounds 1 and 3 were utilized as leads for optimization with efficacy in mFPT upon oral dosing, low to moderate permeability, and

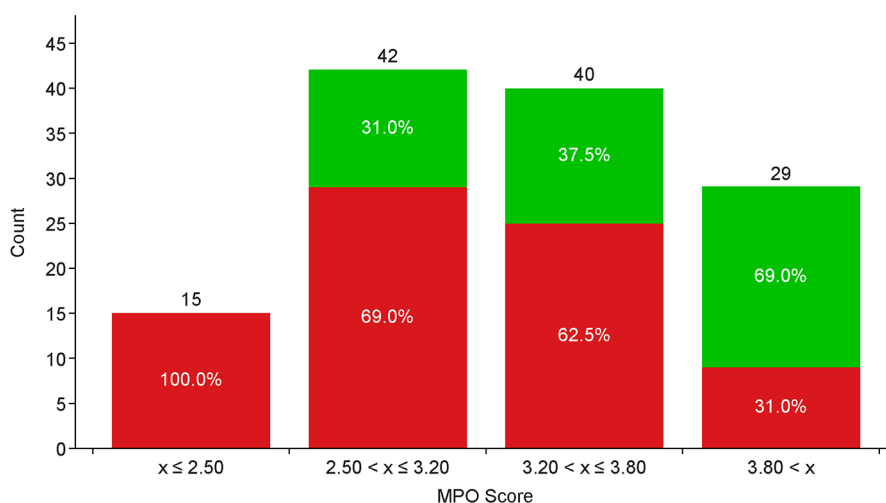


Figure 3. Categorical enrichment in rat oral bioavailability as a function of MPO score (%F \geq 20%, green; %F < 20%, red).

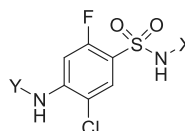
limited selectivity over Na_v1.6. Analogue designs were prioritized for synthesis through MPO evaluation and breakthroughs in selectivity over Na_v1.6, which could be rationalized via homology modeling (vide infra).

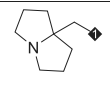
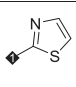
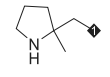
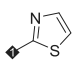
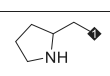
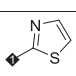
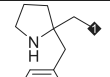
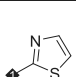
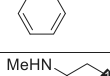
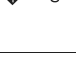
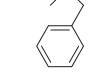
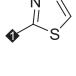
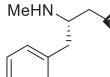
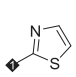
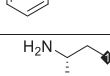
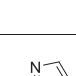
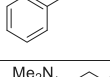
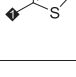
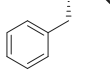
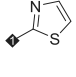
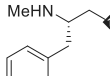
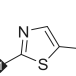
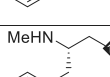
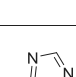
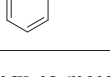
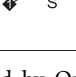
Starting with compound **3**, opening the [3.3.0] ring system to a pyrrolidine scaffold afforded analogues **4** through **7**, which significantly reduced Na_v1.7 potency including inactive compounds **6** and **7** (Table 2). Compound **5** was screened for rat pharmacokinetics (PK) and had bioavailability of 14%, consistent with the enrichment for a compound with an MPO of 3.2. Addition of a phenyl ring to compound **5** yielded **8**, with a 5-fold improvement in Na_v1.7 potency, and importantly, moderate selectivity over Na_v1.6. While this analogue had an MPO score of 4.0, bioavailability was only 7%, likely due to high rat clearance ($CL_{int} = 5830$) potentially due to metabolism.¹³ The pyrrolidine ring was opened to afford **9** and **10**, with reduced Na_v1.7 potency but maintained moderate selectivity over Na_v1.6 for compound **10**. Surprisingly, removing the quaternary center affording **11** increased potency compared to **10** and increased selectivity over Na_v1.6 to more than 100-fold. The MPO score of 4.0 for **11** translated to 25% oral bioavailability despite high clearance. Removal of the methyl group from the terminal amine to afford **12** lost all Na_v1.7 potency, and addition of a methyl group (**13**) also reduced on-target potency by 4-fold. Despite the promising selectivity PK profile for compound **11**, the 2-aminothiazole sulfonamide was still a risk for potential toxicity via known metabolic activation pathways, which were observed in rat and human microsomal incubations.¹⁴ A survey of thiazole replacements that would reduce the potential for metabolic activation revealed very limited options without compromising on target potency.¹⁵ Fluorothiazole **14** maintained the overall profile of **11** regarding potency, selectivity, and oral bioavailability while also having the potential to diminish oxidative metabolism on the thiazole ring.¹⁶ Thiadiazole **15** also had the potential to reduce oxidative metabolism as on the sulfonamide aryl ring, however, potency and MPO score were reduced through this design element. While **14** was considered a promising new lead, clearance was significantly higher compared with initial lead **3**, potentially due to incorporation of the phenyl ring, which increased lipophilicity and offered additional opportunity for metabolism. To further optimize

this lead, isosteric replacements for the phenyl ring in **14** were explored.

Replacing the phenyl substituent with cycloalkyl motifs afforded analogues **16** and **17**, which both reduced Na_v1.7 potency 4- and 14-fold, respectively, as well as reduced MPO score (via reduced lipophilicity; $cLogD < 1.5$ for each) and permeability as shown in Table 3. Notably, cyclopropane **17** significantly lowered clearance compared to **14** or **16** and maintained excellent oral bioavailability, suggesting that increasing sp^3 character could improve PK profiles in the series. Incorporation of a quaternary methyl group in **18** restored potency to within 2-fold of lead **14** and increased permeability. Opening the cyclopropane ring to afford the *tert*-butyl motif in **19** resulted in slightly improved potency compared to **14**, high MPO score, moderate permeability and selectivity, and excellent rat bioavailability. Utilizing **19** as design inspiration, trimethylsilyl analogue **20** provided the most potent Na_v1.7 blocker to date in the series with moderate selectivity over Na_v1.6, reduced clearance, and good bioavailability.¹⁷ As a known phenyl isostere, the bicyclo[1.1.1]pentane was targeted, providing **21** with desired potency and selectivity, but increased clearance was observed; for this reason, **21** was not characterized further. Compound **19** provided improved selectivity over Na_v1.6, permeability, and bioavailability compared to initial lead compound **3** and was selected as an exemplar in the series for further characterization.

An interesting observation was made that compound **19** is essentially an open form of lead compound **1** that increased selectivity over Na_v1.6. To explore this selectivity phenomenon, compounds **1** and **19** were docked to the binding site with Glide v7.7 of Schrödinger¹⁸ software using a known X-ray crystal structure (PDB 5EK0) containing the human Na_v1.7 binding site for the arylsulfonamide class of inhibitors (top of S1–S4 in domain 4 of the channel).¹⁹ Also, a homology model of Na_v1.6 VSD4 was built using Prime in Maestro v11.4.²⁰ Then, a 100 ns molecular dynamics (MD) simulation was performed for both compounds **1** and **19** in Na_v1.7 and Na_v1.6 in the presence of explicit water and membrane using Desmond v5.2. Last, 400 snapshots of each simulation were used to estimate binding free energy using prime_mmgbsa in Maestro v11.4. The results were shown in Figure 4.

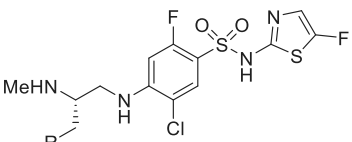
Table 2. Western SAR and Selectivity over Na_v1.6


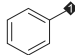
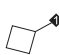



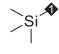

Compound	Y	X	Na _v 1.7 IC ₅₀ (nM) ^a	Na _v 1.6 IC ₅₀ (nM) ^a	MPO Score / Rat %F	P _{app} (10 ⁻⁶ cm/s) ^b	In vivo Rat CL _{int} ^c
3			120	60	3.5 / 40	2	210
4 (R or S)			2970	2080	3.2 / ND	ND	ND
5 (S or R)			900	860	3.2 / 14	ND	400
6 (R or S)			> 34000	> 34000	3.0 / ND	ND	ND
7 (S or R)			> 34000	> 34000	3.0 / ND	ND	ND
8 (R or S)			25	420	4.0 / 7	13	5830
9 (R or S)			> 34000	> 34000	4.0 / ND	ND	ND
10 (S or R)			1140	> 34000	4.0 / ND	ND	ND
11			240	> 34000	4.0 / 25	10	4820
12			> 34000	> 34000	2.8 / ND	ND	ND
13			850	> 34000	4.0 / ND	ND	ND
14			400	> 34000	4.0 / 63	8	3020
15			1090	> 34000	3.4 / ND	ND	ND

^aEstimated hyperpolarized state potency as measured by Qube in HEK293 cells stably expressing human Na_v1.7 or Na_v1.6; IC₅₀ values are estimated from ≥3 cellular measurements at varying compound concentrations and standard deviation <50% of average value shown. ^bMonolayer assay in MDCK cells. ^cRat CL_{int} = (84 × rat CL) / [rat f_u × (84 - rat CL)]; units mL/min/kg; IV, 0.05 mpk cassette dosing or 2 mpk single dosing in DMSO/PEG400/water (20/60/20); PO, 10 mpk in PEG400/Tween90/water (40/10/50).

Not surprisingly, several key interactions were maintained between the two compounds: interaction of the acidic sulfonamide with R1608, terminal basic amine interaction with D1586, and key π - π stacking interaction with Y1537 (not labeled, but central in Figure 4) with the aromatic core of the molecule. The MD simulation also provided slight differences in docked versions of **19** and **1**, namely the *tert*-butyl motif in **19** reached higher into the binding pocket toward the top or loop region of S2, where several amino acid residue differences were observed between human Na_v1.7 and Na_v1.6 (Q1530K and T1590K shown; others removed for clarity). Steric clashes

between **19** and the larger amino acid residues in Na_v1.6 could underly the difference in selectivity. Relative binding free energy calculations were also performed for both **1** and **19** using the MM_GBSA method. Compound **19** was calculated to bind approximately 2 kcal/mol more strongly to Na_v1.7 than Na_v1.6, while compound **1** was predicted to have similar binding energy between the two channels, consistent with the selectivity profiles of both compounds. It should be noted that the standard deviations were overlapping these differences, however, this methodology might represent a prospective

Table 3. Phenyl Replacements and Selectivity over Na_v1.6


Compound	R	Nav1.7 IC ₅₀ (nM) ^a	Nav1.6 IC ₅₀ (nM) ^a	MPO Score / Rat %F	P _{app} (10 ⁻⁶ cm/s) ^b	In vivo Rat CL _{int} ^c
14		400	> 34000	4.0 / 63	8	3020
16		1780	> 34000	3.8 / ND	5	8090
17		5540	> 34000	3.4 / 78	3	380
18		720	> 34000	3.8 / 94	7	830
19		300	18700	4.0 / 100	8	1670
20		44	3130	3.9 / 74	ND	500
21		120	> 34000	3.7 / ND	10	2300

^aEstimated hyperpolarized state potency as measured by Qube in HEK293 cells stably expressing human Na_v1.7 or Na_v1.6; IC₅₀ values are estimated from ≥3 cellular measurements at varying compound concentrations and standard deviation <50% of average value shown. ^bMonolayer assay in MDCK cells. ^cRat CL_{int} = (84 × rat CL) / [rat f_u × (84 - rat CL)]; units mL/min/kg; IV, 0.05 mpk cassette dosing or 2 mpk single dosing in DMSO/PEG400/water (20/60/20); PO, 10 mpk in PEG400/Tween90/water (40/10/50).

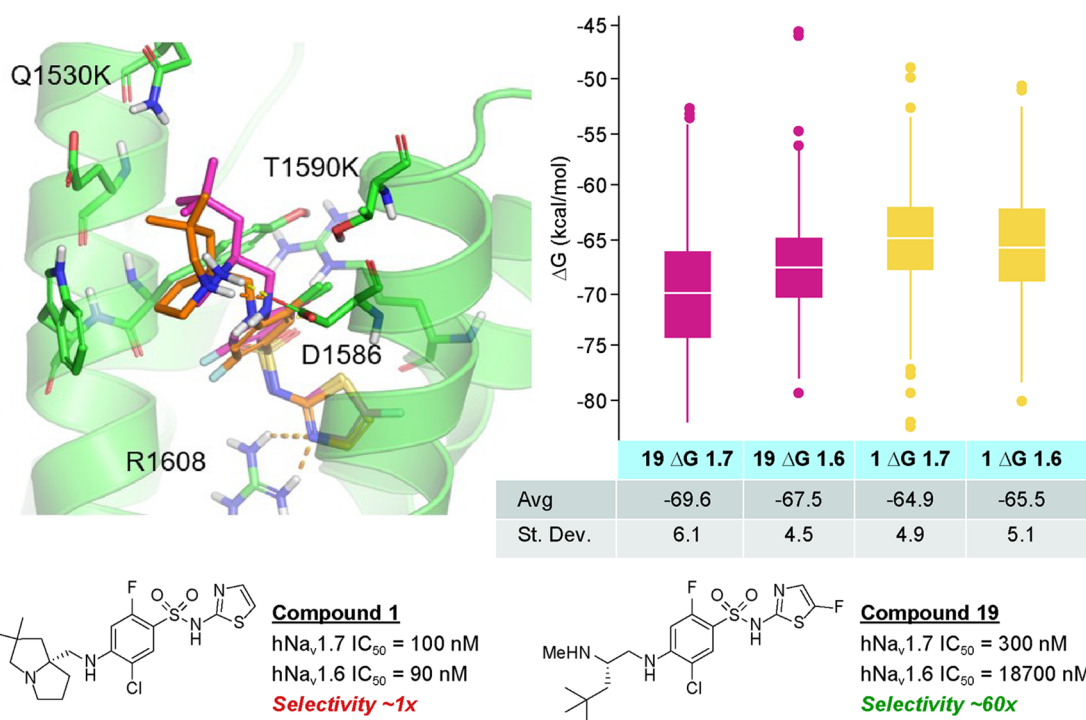
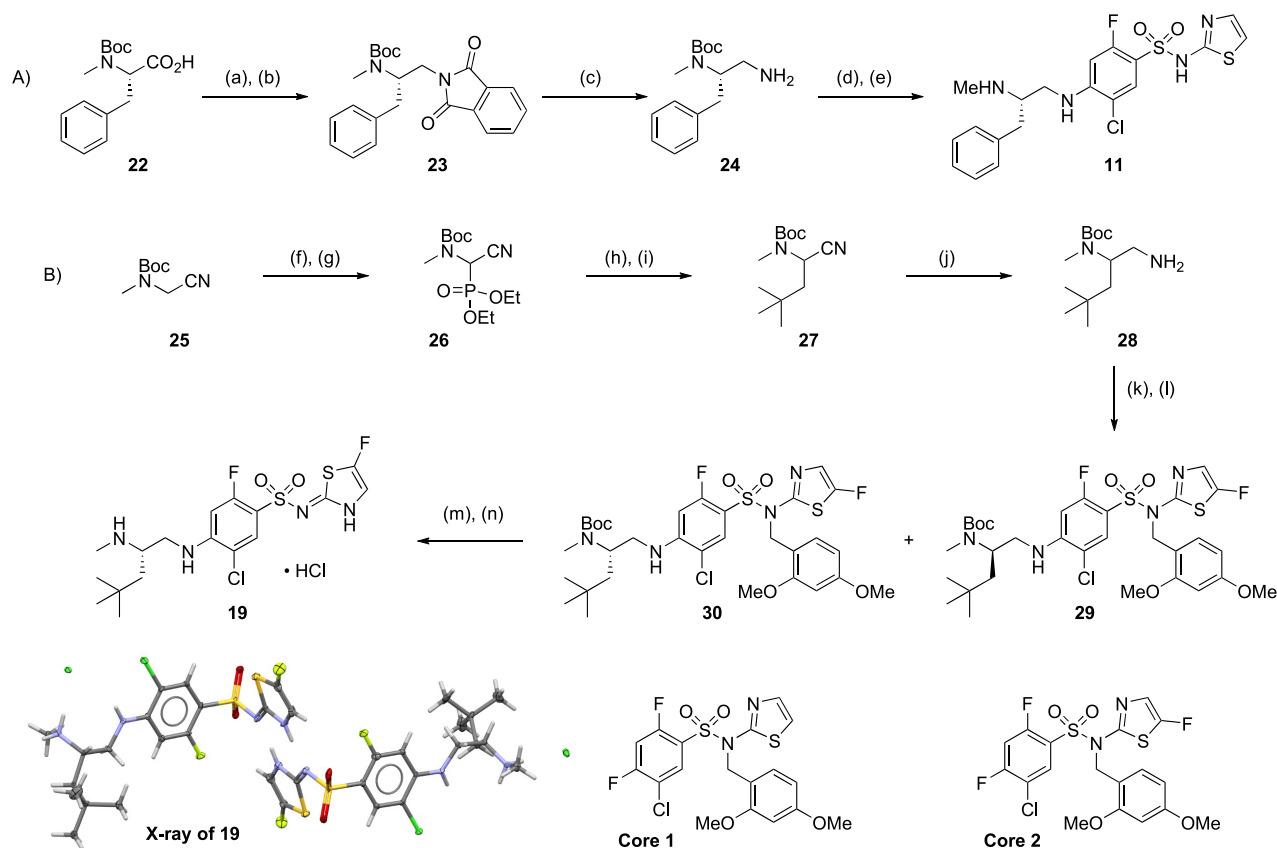


Figure 4. Docked models and binding free energy calculations for 1 and 19 in hNav1.7 and hNav1.6.

Scheme 1. Synthesis of Compounds 11 (A) and 19 (B)^a

^aReagents and reaction conditions: (A) (a) $\text{BH}_3 \cdot \text{THF}$, THF, 0–25 °C, 0.5 h, 97%; (b) phthalimide, DTAD, PS-PPh_3 , THF, 25 °C, 0.5 h, 78%; (c) hydrazine hydrate, MeOH, reflux, 2 h, 97%; (d) core 1, Hunig's base, NMP, 100 °C, microwave, 20 min, 77%; (e) TFA, DCM, 25 °C, 3 h, 79%. (B) (f) *N*-bromosuccinimide, CCl_4 , 80 °C, 2 h, 96%; (g) triethylphosphite, THF, 75 °C, 16 h, 98%; (h) pivaldehyde, tetramethylguanidine, THF, –78 to 25 °C, 9 h, 57%; (i) NaBH_4 , MeOH, 25 °C, 2 h, 64%; (j) Raney nickel, H_2 , EtOH, 25 °C, 2 h, 63%; (k) core 2, TEA, DMF, 25 °C, 16 h, 83%; (l) SFC separation, Chiralpak AD-3 150 mm \times 4.6 mm I.D.; mobile phase, 2-propanol (0.05% DEA) in CO_2 from 5% to 40%; flow rate, 2.4 mL/min; wavelength, 220 nm; enantiomer 1 = 30 (R_t = 5.0 min), enantiomer 2 = 29 (R_t = 5.4 min); (m) TFA, DCM, 25 °C, 1 h; (n) reverse phase HPLC (acetonitrile/0.05% HCl in water), 61% over 2 steps.

method to prioritize analogue designs based on potential for increased selectivity over $\text{Na}_v1.6$.

Representative synthetic routes to the compounds above are described in Scheme 1. The synthesis of compound 11 began with a borane reduction of *N*-Boc-*N*-methyl-*L*-phenylalanine (22) followed by Mitsunobu with phthalimide to afford 23. Phthalimide removal afforded 24, which underwent an $\text{S}_{\text{N}}\text{Ar}$ with core 1 and acidic deprotection to afford 11. The synthesis of 19 began with the bromination/phosphonate sequence from 25 to afford 26. Horner–Wadsworth–Emmons olefination with pivaldehyde followed by conjugate reduction afforded 27 in modest yield. Reduction with Raney nickel and hydrogen afforded 28, which was engaged in an $\text{S}_{\text{N}}\text{Ar}$ reaction with core 2, which afforded 29 and 30 after chiral separation. Deprotection of 30 afforded the hydrochloride salt of 19.²¹ The identity and absolute stereochemistry of 22 was determined by X-ray crystallography.²²

Compound 19 underwent additional profiling prior to in vivo evaluation for pain efficacy and target modulation. In preparation for these studies, manual electrophysiology (EP) experiments were performed using the hyperpolarized assay protocol, and potency values were found to be within 3-fold of screening potency values with recapitulation of selectivity profiles over $\text{Na}_v1.6$ (60-fold) and limited activity on $\text{Na}_v1.5$

(Table 4). The potency of 19 was right-shifted on mouse $\text{Na}_v1.7$ (IC_{50} = 8.8 μM) and less right-shifted in rhesus experiments (IC_{50} = 310 nM) compared to human potency consistent with previously evaluated compounds in the series. The physicochemical properties of 19 are within targeted MPO ranges that resulted in high rat bioavailability. This analogue was also a substrate for human and rat P-glycoprotein (Pgp) efflux transporters and, consistent with this finding, limited central penetration was observed upon oral dosing in mice, with a CSF-to-unbound plasma ratio of 0.02. This zwitterionic analogue had good kinetic solubility under low and neutral pH conditions, had limited CYP inhibition potency against three major isoforms, moderate PXR activation potential, and no significant activity in broad off-target profiling. Pharmacokinetics in dog revealed low clearance, a 6 h half-life, and moderate oral bioavailability. Rhesus bioavailability was negligible; however, pharmacokinetics were sufficient to evaluate this compound in our target modulation assay via IV administration. Finally, metabolic profiling in human, rat, dog, and rhesus hepatocytes revealed *N*-demethylation (metabolite potency; $\text{hNa}_v1.7$ IC_{50} = 3.5 μM) as the major route of metabolism with no metabolism of the thiazole motif. This finding suggested that fluorination of

Table 4. Additional Profiling of Compound 19^d

property	compd 19
human Na _v 1.7/1.6/1.5 IC ₅₀ [nM] (fold-selectivity) ^a	87/5230 (60×)/ >34000 (>390×)
mouse/rhesus Na _v 1.7 IC ₅₀ (nM) ^a	8800/310
mouse/rhesus/human PPB	94%/98%/98%
MW/HBD/log D ^c /PSA	453 g/mol/3/1.7/89 Å ²
Pgp (BA/AB ratio; h/r)	4.9/>14
mouse brain/plasma/CSF (μM) ^e	0.1/4.9/0.005
pK _a (sulfonamide/amine)	5.4/9.0
solubility (pH 2, 7) ^b	170, 148 μM
CYP IC ₅₀ (3A4/2C9/2D6, μM)	>50, 28, 20
PXR EC ₅₀ (μM)/% max	10/80%
Panlabs (97 assays)	no hits <10 μM
rat PK: CL, CL _{int} , V _{dss} , T _{1/2} , F ^f	29, 1670, 2.1, 2.5, 100%
dog PK: CL, CL _{int} , V _{dss} , T _{1/2} , F ^f	4.5, 200, 0.8, 6.0, 25%
rhesus PK: CL, CL _{int} , V _{dss} , T _{1/2} , F ^f	11, 610, 0.3, 1.3, 2%

^aEstimated hyperpolarized protocol inhibition potency as measured by manual electrophysiology in HEK293 cells stably expressing human, rhesus, or mouse Na_v1.7; IC₅₀ values are estimated from ≥3 cellular measurements at varying compound concentrations and standard deviation <50% of average value shown. ^bMSD HPLC kinetic solubility assay. ^cMSD HPLC log D assay. ^dMonolayer assay in MDCK cells. ^e100 mpk PO, 1.25 h sampling. ^fCL_(int) units = mL/min/kg, V_{dss} = L/kg, T_{1/2} = hours.

the thiazole reduced the potential metabolic liability of the aminothiazole sulfonamide.

To estimate pain efficacy in a rodent behavioral pain assay, compound 19 was evaluated in the mFPT assay and administered orally to mice at three dose levels 15 min prior to formalin injection (Figure 5).²³ Plasma sampling was performed 1.5 h after compound administration to coincide with T_{max} values provided by satellite PK experiments. Limited reversal of the phase 1 (acute phase) effects of formalin administration were observed at all three dose levels. Significant and full reversal of these effects were observed in phase 2 (tonic phase) of the experiment, with unbound concentrations at EC₉₀ of 360 nM. This represents a ratio of 0.04 (360/8800 nM) when normalizing for mouse potency. Although outliers of this magnitude were observed in Figure 1, this result was surprising given the correlation previously acquired, with most compounds demonstrating approximately a ratio unity comparing mouse hyperpolarized Na_v1.7 potency

and unbound concentration for full mFPT efficacy. To investigate further, the team decided to assess target modulation orthogonally in a model of rhesus olfaction to further assist with the determination of target concentration for human efficacy.

Loss-of-function mutations in Na_v1.7 not only cause insensitivity to painful stimuli but also cause anosmia (lack of sense of smell) through inactivation of Na_v1.7 in the olfactory bulb.²⁴ A target modulation assay was developed using functional magnetic resonance imaging (fMRI) to measure odorant-induced olfaction in the olfactory bulb (OB) of anesthetized rhesus monkeys (nonhuman primates, or NHPs), previously reported from our laboratories as a potential translative clinical biomarker.^{25,26} Briefly, the study was performed with with NHPs each for vehicle control and for compound 19. The fMRI measurement paradigm for odorant-induced olfaction was 1 min for baseline, 1 min for odor stimulation, and 2 min for recovery (4 min total for each fMRI measurement). Thirty fMRI measurements were made for each NHP during a 2 h period. Compound 19 or vehicle delivery was started 1 h after acquisition of data and was continuously infused for the following hour. The strength of fMRI response was quantified by averaging the amplitudes of fMRI signals during the stimulation period. The inhibition on the olfaction was expressed as percentage inhibition of the strength of fMRI response in the control period. Time courses of fMRI signals in olfactory bulb upon a 40 s odor administration (isoamyl acetate: red bars) before/after the vehicle, and compound 19 delivery are shown in parts A and B of Figure 6, respectively. With the vehicle administration, the odorant-induced fMRI activations in the OB are similar before and after the administration, indicating that the vehicle has no significant effect on the olfaction. The odorant-induced fMRI activations in the OB after the administration of 19 were weaker than the fMRI responses before the administration, suggesting that the compound 19 inhibits the odorant-induced olfaction in the NHPs with statistical significance (Figure 6C).

Compound 19 reduced olfactory response by approximately 35%, with an unbound plasma concentration of 1.5 μM and a ratio compared to rhesus potency of 4.8 (1500/310 nM). These results were more consistent with previous compounds studied that demonstrated that full efficacy in mFPT correlated to approximately a 40% reduction in rhesus olfactory response at unbound concentrations approximately equivalent to Na_v1.7

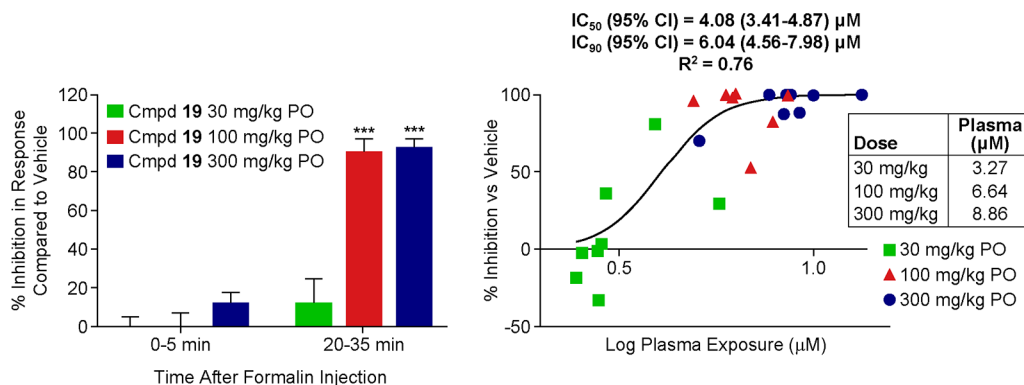


Figure 5. Oral efficacy of compound 19 in mouse formalin paw test. Measurement of formalin-induced nociceptive behaviors in mice (C57BL/6 mice) following administration of vehicle (10% Tween 80; dose volume = 5 mL/kg) or rising oral doses of compound 19. Compound 19 was administered 15 min prior to formalin injection and plasma concentrations were evaluated 1.5 h postadministration. Data were analyzed using within-subject ANOVA to determine main effects and 1 sample *t* test to compare to vehicle (*N* = 8/group); ****P* > 0.001.

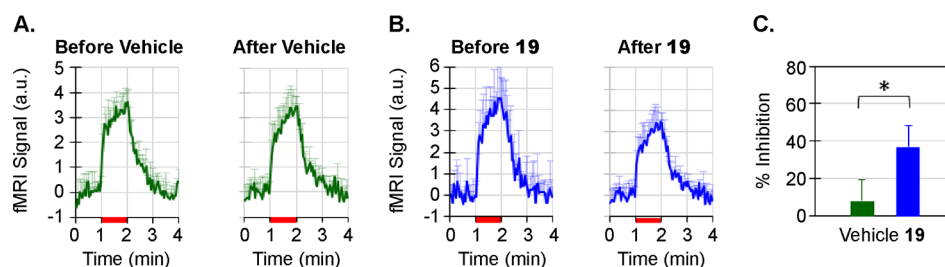


Figure 6. Target modulation efficacy of compound **19** in rhesus olfaction fMRI. Measurement of odorant-induced olfaction in the olfactory bulb of NHPs following administration of vehicle (30% Captisol, dose volume = \sim 8 mL/animal) or compound **19** (19.2 mg/kg). (A) Time courses of fMRI signals which represent the odorant-induced olfaction in the OB of NHPs before and after vehicle administration (mean \pm STD, $n = 4$). (B) Time courses of fMRI signals before and after compound **19** (C'22) administration (mean \pm STD, $n = 4$). (C) Compare the inhibition by compound **22** and the effect from the vehicle ("*" statistical student t test, $P < 0.012$). Red bars in (A,B): odorant stimulations.

potency.²⁷ These disparate behavioral efficacy, mFPT overall correlations and target modulation data made it difficult to project an appropriate dose estimate for efficacy in clinical evaluation. The team chose to bracket human dose predictions using the three efficacy or target modulation data sets. [Table 5](#)

Table 5. Estimated Human Dose Projections Based on Changing C_{trough} Targets of Compound **19**

C_{trough} target	regimen	dose (mg)
0.04 \times $\text{Na}_v1.7$ IC_{50}	BID	40
1 \times $\text{Na}_v1.7$ IC_{50}	BID	960
4.8 \times $\text{Na}_v1.7$ IC_{50}	BID	4600

displays the estimated BID ("bis en die" or dosing twice per day) human dose projections via allometric scaling for **19** using the three end points to set trough concentration efficacy targets in man.²⁸ While dose projections from behavioral efficacy and IVIC studies were considered clinically feasible (40–960 mg BID), accessing the top end of the efficacy curve set by rhesus olfaction (4.6 g BID) would likely not be possible. This data suggested the need for significant additional optimization toward clinical candidate identification to confidently interrogate $\text{Na}_v1.7$ as a therapeutic target.

In conclusion, a correlation was established between hyperpolarized $\text{Na}_v1.7$ and $\text{Na}_v1.6$ assay protocols to efficacy and off-target end points: behavioral pain efficacy and target modulation for $\text{Na}_v1.7$ and respiratory side effects for $\text{Na}_v1.6$. A novel MPO paradigm was developed to enrich design cycles for analogues with adequate rodent bioavailability concomitant with selectivity optimization. This strategy afforded analogues with a more than 100-fold selectivity over $\text{Na}_v1.6$ with high rodent oral bioavailability. Molecular dynamics simulations and free energy binding calculations were performed, which provided rationale for selectivity differences between structurally related compounds. These tools could potentially be utilized for prospective design of analogues with increased potency, selectivity, and oral bioavailability. An exemplar compound (**19**) has demonstrated behavioral pain efficacy in mFPT and target modulation in a rhesus olfaction fMRI assay, however, dose predictions for leading analogues suggest the need for significant optimization toward candidate selection to adequately test the mechanism. Future efforts will focus on the identification of analogues with more aligned ratios in pain efficacy and target modulation compared to potency and reduction of predicted dose estimates via potency and PK optimization. These efforts will be reported in due course.

■ ASSOCIATED CONTENT

Supporting Information

The Supporting Information is available free of charge at <https://pubs.acs.org/doi/10.1021/acsmchemlett.1c00218>.

Synthetic procedures; assay protocols; MPO calculation methods; X-ray crystallographic data; compound characterization data ([PDF](#))

Roecker $\text{Na}_v1.7$ ACS MCL spectra ([PDF](#))

■ AUTHOR INFORMATION

Corresponding Author

Anthony J. Roecker – Discovery Chemistry, Merck & Co., Inc., West Point, Pennsylvania 19486, United States;

orcid.org/0000-0002-7688-7651;

Email: anthony_roecker@merck.com

Authors

Mark E. Layton – Discovery Chemistry, Merck & Co., Inc., West Point, Pennsylvania 19486, United States

Joseph E. Pero – Discovery Chemistry, Merck & Co., Inc., West Point, Pennsylvania 19486, United States; Present Address: (J.E.P.) GlaxoSmithKline, 1250 South Collegeville Road, Collegeville, Pennsylvania, 19426;

orcid.org/0000-0003-2674-4713

Michael J. Kelly, III – Discovery Chemistry, Merck & Co., Inc., West Point, Pennsylvania 19486, United States

Thomas J. Greshock – Discovery Chemistry, Merck & Co., Inc., West Point, Pennsylvania 19486, United States;

orcid.org/0000-0002-3313-9733

Richard L. Kraus – Pharmacology, Merck & Co., Inc., West Point, Pennsylvania 19486, United States

Yuxing Li – Pharmacology, Merck & Co., Inc., West Point, Pennsylvania 19486, United States

Rebecca Klein – Pharmacology, Merck & Co., Inc., West Point, Pennsylvania 19486, United States

Michelle Clements – Pharmacology, Merck & Co., Inc., West Point, Pennsylvania 19486, United States

Christopher Daley – Pharmacology, Merck & Co., Inc., West Point, Pennsylvania 19486, United States

Aneta Jovanovska – Pharmacology, Merck & Co., Inc., West Point, Pennsylvania 19486, United States

Jeanine E. Ballard – Pharmacokinetic, Pharmacodynamics, and Drug Metabolism, Merck & Co., Inc., West Point, Pennsylvania 19486, United States

Deping Wang – Computational and Structural Chemistry, Merck & Co., Inc., West Point, Pennsylvania 19486, United States

Fuqiang Zhao – Translational Imaging and Biomarkers, Merck & Co., Inc., West Point, Pennsylvania 19486, United States

Andrew P. J. Brunskill – Molecular and Materials Characterization, Merck & Co., Inc., Rahway, New Jersey 07065, United States

Xuanjia Peng – HitS Unite, WuXi AppTec Co., Ltd. (Shanghai), Shanghai 200131, China; orcid.org/0000-0001-6067-0311

Xiu Wang – IDUSU, WuXi AppTec Co., Ltd. (Shanghai), Shanghai 200131, China

Haiyan Sun – IDUSU, WuXi AppTec Co., Ltd. (Shanghai), Shanghai 200131, China

Andrea K. Houghton – Pharmacology, Merck & Co., Inc., West Point, Pennsylvania 19486, United States

Christopher S. Burgey – Discovery Chemistry, Merck & Co., Inc., West Point, Pennsylvania 19486, United States

Complete contact information is available at:

<https://pubs.acs.org/10.1021/acsmchemlett.1c00218>

Author Contributions

All authors have given approval to the final version of the manuscript. Conceived and designed experiments: A.J.R., M.E.L., J.E.P., D.W., F.Z., R.K., R.L.K., A.K.H., and C.S.B. Designed compounds and/or contributed to synthetic route design: A.J.R., M.E.L., J.E.P., M.J.K., III, T.G., X.P., X.W., and H.S. Analyzed data: R.L.K., Y.L., M.C., C.D., A.J., J.B., and D.W. Wrote the paper: A.J.R., D.W., and F.Z. Edited the paper: C.S.B. and M.E.L.

Notes

The authors declare the following competing financial interest(s): The authors are or were employees of Merck and Co., Inc. during the period of this work, and may hold stock in those companies.

ACKNOWLEDGMENTS

We thank Justin Newman for small-molecule X-ray support. We also thank Wilfredo Pinto for high-resolution mass spectrometry support.

ABBREVIATIONS

CNS, central nervous system; SAR, structure–activity relationship; HBD, hydrogen bond donor; cLogD, calculated water/octanol partition coefficient at pH 7.4; PK, pharmacokinetics; PSA, polar surface area; SNAr, nucleophilic aromatic substitution; THF, tetrahydrofuran; MeOH, methanol; DTAD, di-*tert*-butylazodicarboxylate; NMP, *N*-methylpyrrolidinone; TFA, trifluoroacetic acid; DCM, dichloromethane; EtOH, ethanol; TEA, triethylamine; DMF, dimethylformamide; PS, polymer-supported; CL_{int} , intrinsic clearance; mFPT, mouse formalin paw test; NHP, nonhuman primate; MPO, multiparameter optimization; fMRI, functional magnetic resonance imaging; IVIVC, *in vitro*–*in vivo* correlation; BID, “bis in die” or dosing twice per day; PPB, plasma protein binding

REFERENCES

(1) (a) Garland, E. L. Treating chronic pain: the need for non-opioid options. *Expert Rev. Clin. Pharmacol.* **2014**, *7*, 545–550. (b) Dib-Hajj, S. D.; Waxman, S. G. Translational pain research: lessons from genetic and genomics. *Sci. Transl. Med.* **2014**, *6*, 249sr4. (c) Chang, D. S.; Raghavan, R.; Christiansen, S.; Cohen, S. P. *Curr.*

Opin. Anaesthesiol. **2015**, *28*, 379–397. (d) Busserolles, J.; Lolognier, S.; Kerckhove, N.; Bertin, C.; Authier, N.; Eschaliere, A. Replacement of current opioid drugs focusing on MOR-related strategies. *Pharmacol. Ther.* **2020**, *210*, 107519. (e) Time Staff Writers. The Opioid Diaries. *Time Magazine*, March 5, **2018**, <https://time.com/5170231/the-opioid-diaries/>.

(2) (a) Dib-Hajj, S. D.; Yang, Y.; Black, J. A.; Waxman, S. G. The Na_v1.7 sodium channel: from molecule to man. *Nat. Rev. Neurosci.* **2013**, *14*, 49–62. (b) Dib-Hajj, S. D.; Rush, A. M.; Cummins, T. R.; Waxman, S. G. Mutation in the sodium channel 1.7 underlie inherited erythromelalgia. *Drug Discovery Today: Dis. Mech.* **2006**, *3*, 343–350. (c) Faber, C. G.; Hoeijmakers, J. G.; Ahn, H. S.; Cheng, X.; Han, C.; Choi, J. S.; Estacion, M.; Lauria, G.; Vanhoutte, E. K.; Gerrits, M. M.; Dib-Hajj, S.; Drenth, J. P.; Waxman, S. G.; Merkies, I. S. Gain of function Na_v1.7 mutations in idiopathic small fiber neuropathy. *Ann. Neurol.* **2012**, *71*, 26–39. (d) Goldberg, Y. P.; MacFarlane, J.; MacDonald, M. L.; Thompson, J.; Dube, M.-P.; Mattice, M.; Fraser, R.; Young, C.; Hossain, S.; Pape, T.; Payne, B.; Radomski, C.; Donaldson, G.; Ives, E.; Cox, J.; Youngusband, H. B.; Green, R.; Duff, A.; Boltshauser, E.; Grinspan, G. A.; Dimon, J. H.; Sibley, B. G.; Andria, G.; Toscano, E.; Kerdraon, J.; Bowsher, D.; Pimstone, S. N.; Samuels, M. E.; Sherrington, R.; Hayden, M. R. Loss-of-function mutations in the Na_v1.7 gene underlie congenital indifference to pain in multiple human populations. *Clin. Genet.* **2007**, *71*, 311–319. (e) Gingras, J.; Smith, S.; Matson, D. J.; Johnson, D.; Nye, K.; Couture, L.; Feric, E.; Yin, R.; Moyer, B. D.; Peterson, M. L.; Rottman, J. B.; Beiler, R. J.; Malmberg, A. B.; McDonough, S. I. Global Na_v1.7 knockout mice recapitulate the phenotype of human congenital indifference to pain. *PLoS One* **2014**, *9*, e105895.

(3) (a) McKerrall, S. J.; Sutherlin, D. P. Na_v1.7 inhibitors for the treatment of chronic pain. *Bioorg. Med. Chem. Lett.* **2018**, *28*, 3141–3149. (b) Swain, N. A.; Batchelor, D.; Beaudoin, S.; Bechle, B. M.; Bradley, P. A.; Brown, A. D.; Brown, B.; Butcher, K. J.; Butt, R. P.; Chapman, M. L.; Denton, S.; Ellis, D.; Galan, S. R. G.; Gaulier, S. M.; Greener, B. S.; de Groot, M. J.; Glossop, M. S.; Gurrell, I. K.; Hannam, J.; Johnson, M. S.; Lin, Z.; Markworth, C. J.; Marron, B. E.; Millan, D. S.; Nakagawa, S.; Pike, A.; Printzenhoff, D.; Rawson, D. J.; Ransley, S. J.; Reister, S. M.; Sasaki, K.; Storer, R. I.; Stuppel, P. A.; West, C. W. Discovery of clinical candidate 4-[2-(5-amino-1H-pyrazol-4-yl)-4-chlorophenoxy]-5-chloro-2-fluoro-*N*-1,3-thiazol-4-ylbenzenesulfonamide (PF-05089771): design and optimization of diary ether aryl sulfonamides as selective inhibitors of Na_v1.7. *J. Med. Chem.* **2017**, *60*, 7029–7042. (c) Graceffa, R. F.; Boezio, A. A.; Able, J.; Altmann, S.; Berry, L. M.; Boezio, C.; Butler, J. R.; Chu-Moyer, M.; Cooke, M.; DiMauro, E. F.; Dineen, T. A.; Feric Bojic, E.; Foti, R. S.; Fremeau, R. T., Jr.; Guzman-Perez, A.; Gao, H.; Gunaydin, H.; Huang, H.; Huang, L.; Ilch, C.; Jarosh, M.; Kornecook, T.; Kreiman, C. R.; La, D. S.; Ligutti, J.; Milgram, B. C.; Lin, M. J.; Marx, I. E.; Nguyen, H. N.; Peterson, E. A.; Rescourio, G.; Roberts, J.; Schenkel, L.; Shimanovich, R.; Sparling, B. A.; Stellwagen, J.; Taborn, K.; Vaida, K. R.; Wang, J.; Yeoman, J.; Yu, V.; Zhu, D.; Moyer, B. D.; Weiss, M. M. Sulfonamides as selective Na_v1.7 inhibitors: Optimizing potency, pharmacokinetics, and metabolic properties to obtain atropisomeric quinolinone (AM-0466) that affords robust *in vivo* activity. *J. Med. Chem.* **2017**, *60*, 5990–6017. (d) Sun, S.; Jia, Q.; Zenova, A. Y.; Wilson, M. S.; Chowdhury, S.; Focken, T.; Li, J.; Decker, S.; Grimwood, M. E.; Andrez, J.-C.; Hemeon, I.; Sheng, T.; Chen, C.-A.; White, A.; Hackos, D. H.; Deng, L.; Bankar, G.; Khakh, K.; Chang, E.; Kwan, R.; Lin, S.; Nelkenbrecher, K.; Sellers, B. D.; DiPasquale, A. G.; Chang, J.; Pang, J.; Sojo, L.; Lindgren, A.; Waldbrook, M.; Xie, Z.; Young, C.; Johnson, J. P.; Robinette, C. L.; Cohen, C. J.; Safina, B. S.; Sutherlin, D. P.; Ortwine, D. F.; Dehnhardt, C. M. Identification of selective acyl sulfonamide-cycloalkylether inhibitors of the voltage-gated sodium channel (Na_v) 1.7 with potent analgesic activity. *J. Med. Chem.* **2019**, *62*, 908–927. (e) Rothenberg, M. E.; Tagen, M.; Chang, J. H.; Boyce-Rustay, J.; Friesenhahn, J.; Hackos, D. H.; Hains, A.; Sutherlin, D.; Ward, M.; Cho, W. Safety, tolerability, and pharmacokinetics of GDC-0276, a novel Na_v1.7 inhibitor, in a first-in-human, single- and multiple-dose study in healthy volunteers. *Clin.*

Drug Invest. **2019**, *39*, 873–997. (f) Jones, H. M.; Butt, R. P.; Webster, R. W.; Gurrell, L.; Dzygiel, P.; Flanagan, N.; Fraier, D.; Hay, T.; Iavarone, L. E.; Luckwell, J.; Pearce, H.; Phipps, A.; Segelbacher, J.; Speed, B.; Beaumont, K. Clinical micro-dose studies to explore the human pharmacokinetics of four selective inhibitors of human $\text{Na}_v1.7$ voltage-dependent sodium channels. *Clin. Pharmacokinet.* **2016**, *55*, 875–887. (g) Kornecook, T. J.; Yin, R.; Altmann, S.; Be, X.; Berry, V.; Ilch, C. P.; Jarosh, M.; Johnson, D.; Lee, J. H.; Lehto, S. G.; Ligutti, J.; Liu, D.; Luther, J.; Matson, D.; Ortuno, D.; Roberts, J.; Taborn, K.; Wang, J.; Weiss, M. M.; Yu, V.; Zhu, D. X. D.; Fremeau, R. T., Jr.; Moyer, B. D. Pharmacologic characterization of AMG8379, a potent and selective small molecule sulfonamide antagonist of the voltage-gated sodium channel $\text{Na}_v1.7$. *J. Pharmacol. Exp. Ther.* **2017**, *362*, 146–16. (h) Adams, G. L.; Wang, D.; Sun, C. From spider toxins to therapeutics-developing selective $\text{Na}_v1.7$ peptide inhibitors for pain. *RSC Drug Disc. Series.* **2017**, *59*, 411–437. (i) Safina, B. S.; McKerrall, S. J.; Sun, S.; Chen, C.-A.; Chowdhury, S.; Jia, Q.; Li, J.; Zenova, A. Y.; Andrez, J.-C.; Bankar, G.; Bergeron, P.; Chang, J. H.; Chang, E.; Chen, J.; Dean, R.; Decker, S. M.; DiPasquale, A.; Focken, T.; Hemeon, I.; Khakh, K.; Kim, A.; Kwan, R.; Lindgren, A.; Lin, S.; Maher, J.; Mezeyova, J.; Misner, D.; Nelkenbrecher, K.; Pang, J.; Reese, R.; Shields, S. D.; Sojo, L.; Sheng, T.; Verschoof, H.; Waldbrook, M.; Wilson, M. S.; Xie, Z.; Young, C.; Zabka, T. S.; Hackos, D. H.; Ortwine, D. F.; White, A. D.; Johnson, J. P., Jr.; Robinette, C. L.; Dehnhardt, C. M.; Cohen, C. J.; Sutherlin, D. P. Discovery of acyl-sulfonamide inhibitors GDC-0276 and GDC-310. *J. Med. Chem.* **2021**, *64*, 2953–2966.

(4) (a) McDonnell, A.; Collins, S.; Ali, Z.; Iavarone, L.; Surujbally, R.; Kirby, S.; Butt, R. P. Efficacy of the $\text{Na}_v1.7$ blocker PF-05089771 in a randomized, placebo-controlled, double-blind clinical study in subjects with painful diabetic peripheral neuropathy. *Pain* **2018**, *159*, 1465–1476. (c) Siebenga, P.; van Amerongen, G.; Hay, J. L.; McDonnell, A.; Gorman, D.; Butt, R.; Groeneveld, G. J. Lack of detection of the analgesic properties of PF-05089771, a selective $\text{Na}_v1.7$ inhibitor, using a battery of pain models in healthy subjects. *Clin. Transl. Sci.* **2020**, *13*, 318–324.

(5) Mulcahy, J. V.; Pajouhesh, H.; Beckley, J. T.; Delwig, A.; Du Bois, J.; Hunter, J. C. Challenges and Opportunities for Therapeutics Targeting the Voltage-Gated Sodium Channel Isoform $\text{Na}_v1.7$. *J. Med. Chem.* **2019**, *62*, 8695–8710.

(6) For characterization of the compounds and a general discussion of $\text{Na}_v1.x$ pharmacology, see: Roecker, A. J.; Egbertson, M.; Jones, K. L. G.; Gomez, R.; Kraus, R. L.; Li, Y.; Koser, A. J.; Urban, M. O.; Klein, R.; Clements, M.; Panigel, J.; Daley, C.; Wang, J.; Finger, E. N.; Majercak, J.; Santarelli, V.; Gregan, I.; Cato, M.; Filzen, T.; Jovanovska, A.; Wang, Y. H.; Wang, D.; Joyce, L. A.; Sherer, E. C.; Peng, X.; Wang, X.; Sun, H.; Coleman, P. J.; Houghton, A. K.; Layton, M. E. Discovery of selective, orally bioavailable, N-linked arylsulfonamide $\text{Na}_v1.7$ inhibitors with pain efficacy in mice. *Bioorg. Med. Chem. Lett.* **2017**, *27*, 2087–2093.

(7) (a) Eijkelkamp, N.; Linley, J. E.; Baker, M. D.; Minett, M. S.; Cregg, R.; Werdehausen, R.; Rugiero, F.; Wood, J. N. Neurological perspectives on voltage-gated sodium channels. *Brain* **2012**, *135*, 2585–2612. (b) de Lera Ruiz, M.; Kraus, R. L. Voltage-gated sodium channels: structure, function, pharmacology, and clinical indications. *J. Med. Chem.* **2015**, *58* (18), 7093–7118.

(8) Klein, R. M.; Regan, H.; Regan, C. P.; Kraus, R. L.; Li, Y.; Daley, C.; Clements, M. K.; Greshock, T. J.; Roecker, A. J.; Pero, J. E.; Layton, M. E.; Burgey, C. B.; Henze, D. A.; Houghton, A. K. Association of respiratory failure with inhibition of $\text{Na}_v1.6$ in the phrenic nerve. *J. Exp. Ther. Pharm.* **2020**, submitted.

(9) See Experimental Section for details on electrophysiology assay protocols.

(10) Compound **2** required an estimated 90% inhibition concentration due to the inability to achieve 90% reversal of nociceptive behaviors in phase 2 of the mFPT study. 90% inhibition was modelled from a maximum inhibition of 66% at the oral dose of 30 mg/kg. While $\text{Na}_v1.7$ is assumed to be the isoform responsible for mFPT efficacy, the contribution of $\text{Na}_v1.6$ inhibition cannot be ruled

out. For Figure 1, the equation for a straight line fit is $y = 0.7x + 436$, very close to a $y = x$ fit for IVIVC purposes.

(11) Pero, J. E.; Rossi, M. A.; Lehman, H. D. G. F.; Kelly, M. J.; Mulhearn, J. J.; Wolkenberg, S. E.; Cato, M. J.; Clements, M. K.; Daley, C. J.; Filzen, T.; Finger, E. N.; Gregan, Y.; Henze, D. A.; Jovanovska, A.; Klein, R.; Kraus, R. L.; Li, Y.; Liang, A.; Majercak, J. M.; Panigel, J.; Urban, M. O.; Wang, J.; Wang, Y. H.; Houghton, A. K.; Layton, M. E. Benzoxazolinone aryl sulfonamides as potent, selective $\text{Na}_v1.7$ inhibitors with *in vivo* efficacy in a preclinical pain model. *Bioorg. Med. Chem. Lett.* **2017**, *27*, 2683–2688.

(12) (a) Wager, T. T.; Hou, X.; Verhoest, P. R.; Villalobos, A. Central nervous system multiparameter optimization desirability: Application in drug discovery. *ACS Chem. Neurosci.* **2016**, *7*, 767–775. (b) Gunaydin, H. Probabilistic approach to generating MPOs and its application as a scoring function for CNS drugs. *ACS Med. Chem. Lett.* **2016**, *7*, 89–93. (c) Bagal, S. K.; Bungay, P. J. Minimizing drug exposure in the CNS while maintaining good oral absorption. *ACS Med. Chem. Lett.* **2012**, *3*, 948–950.

(13) While the MPO paradigm was utilized as a prospective prioritization method, pharmacokinetic parameters were also used to rationalize poor rat bioavailability from a mechanistic perspective.

(14) Obach, R. S.; Kalgutkar, A. S.; Ryder, T. F.; Walker, G. S. *In vitro* metabolism and covalent binding of enol-carboxamide derivatives and anti-inflammatory agents sudoxicam and meloxicam: insights into the hepatotoxicity of sudoxicam. *Chem. Res. Toxicol.* **2008**, *21*, 1890–1899.

(15) The published 5- and 6-membered heterocyclic sulfonamides in the $\text{Na}_v1.7$ literature were all surveyed on the compound **11** scaffold, and the only motifs with IC_{50} values $< 2 \mu\text{M}$ are shown in this publication.

(16) While fluorine can often deactivate aromatic rings towards metabolism, this is not always the case: Pan, Y. The dark side of fluorine. *ACS Med. Chem. Lett.* **2019**, *10*, 1016–1019.

(17) While compound **20** was initially more potent than compound **19**, manual electrophysiology experiments determined that both compounds were equipotent inhibitors of human $\text{Na}_v1.7$. This supported the decision to advance compound **19** as an exemplar for further characterization.

(18) All programs in this paragraph provided by Schrodinger, LLC, New York, 2017.

(19) Ahuja, S.; Mukund, S.; Deng, L.; Khakh, K.; Chang, E.; Ho, H.; Shriver, S.; Young, C.; Lin, S.; Johnson, J. P., Jr.; Wu, P.; Li, J.; Coons, M.; Tam, C.; Brillantes, B.; Sampang, H.; Mortara, K.; Bowman, K. K.; Clark, K. R.; Estevez, A.; Xie, Z.; Verschoof, H.; Grimwood, M.; Dehnhardt, C.; Andrez, J.-C.; Focken, T.; Sutherlin, D. P.; Safina, B. S.; Starovasinik, M. A.; Ortwine, D. F.; Franke, Y.; Cohen, C. J.; Hackos, D. H.; Koth, C. M.; Payandeh, J. Structural basis of $\text{Na}_v1.7$ inhibition by an isoform-selective small molecule antagonist. *Science* **2015**, *350*, aac5464.

(20) Wang, D.; Roecker, A. J.; Klein, R.; Clements, M.; Daley, C.; Layton, M. E.; Greshock, T. J.; Kraus, R. L.; Wang, J.; Majercak, J.; Santarelli, V.; Gregan, I.; Houghton, A. K.; Coleman, P. J.; Burgey, C. S. Application of binding site mapping, homology modeling and induced docking to the design of potent and selective $\text{Na}_v1.7$ inhibitors. *Unpublished manuscript*.

(21) For additional synthetic details, please see Roecker, A. J.; Layton, M. E.; Greshock, T. J.; Pero, J. E.; Kelly, M. J., III; Zhang, T. N1-phenylpropane-1,2-diamine compounds with selective activity in voltage-gated sodium channels. World Patent WO2017165204, 75 pp.

(22) The coordinates of the X-ray structural data have been submitted to the Cambridge Structural Database with the deposition number CCDC 2045967.

(23) Mogil, J. S.; Wilson, S. G.; Wan, Y. Assessing nociception in murine subjects. In *Methods in Pain Research*; Kruger, L, Ed.; CRC Press, 2001, Chapter 2.

(24) Heimann, D.; Lotsch, J.; Hummel, T.; Doehring, A.; Oertel, B. G. Linkage between increased nociception and olfaction via SCN9A haplotype. *PLoS One* **2013**, *8*, e68654.

(25) Zhao, F.; Holahan, M. A.; Houghton, A. K.; Hargreaves, R.; Evelhoch, J. L.; Winkelmann, C. T.; Williams, D. S. Functional imaging of olfaction by CBV fMRI in monkeys: insight into the role of olfactory bulb in habituation. *NeuroImage* **2015**, *106*, 364–372.

(26) Zhao, F.; Holahan, M. A.; Wang, X.; Uslaner, J. M.; Houghton, A. K.; Evelhoch, J. L.; Winkelmann, C. T.; Hines, C. D. G. fMRI study of the role of glutamate NMDA receptor in the olfactory processing in monkeys. *PLoS One* **2018**, *13*, e0198395.

(27) Ballard, J. E.; Pall, P.; Vardigan, J.; Zhao, F.; Holahan, M. A.; Kraus, R.; Li, Y.; Henze, D.; Houghton, A.; Burgey, C. S.; Gibson, C. Application of pharmacokinetic-pharmacodynamic modeling to inform translation of *in vitro* Na_v1.7 inhibition to *in vivo* pharmacological response in non-human primate. *Pharm. Res.* **2020**, *37*, 181.

(28) The dose projections were performed using a combination of dog and rat allometry varying the C_{trough} concentrations to match the mFPT, IVIVC average, and rhesus olfaction efficacy end points.